Solar Energy 218 (2021) 525–531

Contents lists available at ScienceDirect

Solar Energy

journal homepage: www.elsevier.com/locate/solener

Stable and efficient Sb_2Se_3 solar cells with solution-processed NiO_x hole-transport layer

Liping Guo [a], S.N. Vijayaraghavan [a], Xiaomeng Duan [a], Harigovind G. Menon [a], Jacob Wall [a], Lingyan Kong [b,c], Subhadra Gupta [a], Lin Li [a], Feng Yan [a,c,*]

[a] Department of Metallurgical and Materials Engineering, The University of Alabama, Tuscaloosa, AL 35487, USA
[b] Department of Human Nutrition and Hospitality Management, The University of Alabama, Tuscaloosa, AL 35487, USA
[c] Alabama Water institute, The University of Alabama, Tuscaloosa, AL 35487, USA

ARTICLE INFO

Keywords:
Sb_2Se_3 solar cells
Hole-transport layer
NiO_x nanoparticles
Spin coating
Stability

ABSTRACT

Sb_2Se_3 is a promising absorber material for thin-film solar cells owing to its earth-abundant and non-toxic constituents, superior optoelectronic properties, and unique one-dimensional crystal structure. To further increase the power conversion efficiency of the Sb_2Se_3, we fabricated an n-i-p structure by integrating a solution-processed NiO_x hole-transport layer (HTL) into Sb_2Se_3 solar cells to enhance the carrier collection. In this study, we systematically screen the thickness of NiO_x HTL and demonstrate an improved average power conversion efficiency from 6.12% to 7.15% with a 50 nm NiO_x HTL. The mechanism associated with the improved device performance was characterized through the microstructure of the material, device physics, and interface electronic behaviors. It is also shown that the low-cost and scalable solution-processed NiO_x HTL can improve device stability under an accelerated stress test. Thus, this work paves a way to further improve the performance of antimony chalcogenides-based solar cells via tailoring the inorganic HTL.

1. Introduction

Photovoltaics (PV, i.e., solar cells) technology offers clean, affordable, and sustainable energy via directly converting sunlight into electricity to address the global energy crisis and alleviate issues associated with burning fossil fuels (Crabtree and Lewis, 2007). From the traditional Si wafer-based technology to the thin-film-based CdTe and CIGS, along with the halide perovskite solar cells, all these PV technologies already demonstrate power conversion efficiency (PCE) of over 22% (Green and Bremner, 2017; Green et al., 2019; Wong et al., 2019). Nevertheless, the rigid nature of Si wafer, the toxicity of Cd, and the high cost of In and Ga, along with the instability of halide perovskite pose challenges for the PV development (Kamruzzaman et al., 2017; Zhou et al., 2014). Recently, Sb_2Se_3 has attracted extensive attention as a light-absorber material for solar cells with a theoretical PCE of ~ 32% based on the Shockley-Queisser limit (Green and Bremner, 2017) due to its superior optoelectronic properties, such as the high absorption coefficient ($>10^5$ cm^{-3}) in the visible region (Zeng et al., 2016), and a suitable bandgap (1.1 ~ 1.2 eV) (Zeng et al., 2016; Zhou et al., 2014; Zhou et al., 2015). Besides, Sb_2Se_3 is a stable and low-toxic binary compound with a stable orthorhombic crystalline phase in ambient air, and thus, it avoids the complex phase control during manufacturing as encountered in CIGS technology and instability of perovskite (Zhou et al., 2014). More importantly, noncubic Sb_2Se_3 is comprised of one-dimensional ribbons $(Sb_4Se_6)_n$ stacked by the weak van der Waals (vdW) (Guo et al., 2018; Zeng et al., 2016; Zhou et al., 2015), where the grain boundaries (GBs) area can be self-passivated without dangling bonds to prevent the common recombination loss due to GBs in typical three-dimensional PV technologies (Guo et al., 2018; Zhou et al., 2015).

So far, the PCE of Sb_2Se_3 solar cell has rapidly improved from less than 1% to 10% within one decade through various growth techniques such as chemical bath deposition (CBD), (Messina et al., 2009) hydrazine (N_2H_4) solution-processed method (Zhou et al., 2014), rapid thermal evaporation (RTE) (Zhou et al., 2015), close-Space Sublimation, (Li et al., 2018; Li et al., 2019b) and hydrothermal deposition method (Tang et al., 2020). Despite the stunning progress made in the area, the efficiency improvement is largely plagued by its open-circuit voltage (V_{OC}) deficit due to the low doping density of Sb_2Se_3 (Chen and Tang, 2020; Chen et al., 2017; Hobson et al., 2020). To address this issue, one strategy is to introduce a hole-transport layer (HTL) to effectively extract

* Corresponding author at: Department of Metallurgical and Materials Engineering, The University of Alabama, Tuscaloosa, AL 35487, USA.
E-mail address: fyan@eng.ua.edu (F. Yan).

https://doi.org/10.1016/j.solener.2021.02.063
Received 16 January 2021; Received in revised form 23 February 2021; Accepted 26 February 2021
Available online 21 March 2021

the photogenerated holes. Previous studies have successfully employed many hole-transport materials into Sb_2Se_3 solar cells. For instance, organic PCDTBT, Spiro-OMeTAD, and P3HT have been reported as hole-transport material (HTM) in Sb_2Se_3 sensitized solar cells, which can improve the device performance significantly (Choi et al., 2014; Guijarro et al., 2012; Ju et al., 2020; Li et al., 2018; Tang et al., 2020). However, these organic HTMs face stability issues. Thus, inorganic HTMs such as colloidal quantum dot (QD) PbS, and CuSCN were introduced to Sb_2Se_3 solar cells (Chen et al., 2017; Li et al., 2019a). However, QD PbS has the issue of the toxicity of Pb and CuSCN may introduce fast diffused Cu into the Sb_2Se_3. Taking all these into consideration, it is of great significance to develop a non-toxic and stable HTM for Sb_2Se_3 solar cells for further performance improvement while maintaining its long-term stability.

Traditionally, NiO_x is an ambient air-stable and nontoxic wide-bandgap p-type HTL, and, it has been successfully demonstrated in high-efficiency perovskite solar cells through the solution process (Lee et al., 2020; Park et al., 2015; Xu et al., 2015; Yin et al., 2016; You et al., 2016; Zhu et al., 2014). As for the antimony chalcogenide solar cells, solution-processed NiO_x nanoparticles show promising hole transport capability in the Sb_2S_3 solar cells (Jin et al., 2018). However, for the Sb_2Se_3 solar cells, there are only limited results using NiO_x, such as thermally evaporated thin NiO_x buffer layer for the Ni back contact development of Sb_2Se_3 solar cells (Zhang et al., 2019). No systematic investigation of the solution-processed NiO_x HTL for the Sb_2Se_3 solar cell has been done yet.

In this paper, we successfully demonstrated the solution-processed NiO_x nanoparticles as an HTL on Sb_2Se_3 thin-film solar cells with improved device performance. We employed a thermal decomposition method to synthesize the NiO_x nanoparticles which were then dispersed in deionized water (DIW) to form NiO_x nanoparticle ink. NiO_x HTL film was then deposited on Sb_2Se_3 film via the spin coating method, where the spinning speed was regulated to control the NiO_x thickness. By tailoring the NiO_x HTL thickness, the champion Sb_2Se_3 solar cell delivered a PCE of 7.29%, with V_{OC} of 0.41 V, J_{SC} of 30.94 mA/cm^2, and *FF* of 57.26%. The improved performance originated from the reduced carrier recombination at the Sb_2Se_3/NiO_x interface due to the NiO_x passivation effect. Moreover, the device with NiO_x HTL maintains improved stability after light soaking for 140 h.

2. Experimental section

2.1. NiO_x nanopowder fabrication and solution preparation

0.05 mol $Ni(NO_3)_2{\cdot}6H_2O$ was dissolved in 10 mL deionized water (DIW). Then NaOH solution was added into the as-dissolved $Ni(NO_3)_2$ solution under vigorous stirring until the solution turned into a turbid green color with a pH of 10. The solution was then filtered to obtain the precipitation which was washed by DIW to get rid of the impurities. This step was repeated at least four times to guarantee the purity of the precipitates. The wet precipitate was dried at 80 °C for 8 h and then ground into powder, which was then annealed in air at 270 °C for 2 h to get the NiO_x nanopowders. NiO_x nanopowders were dissolved into DIW to form an ink of ~ 20 mg/mL concentration. The solution was ultrasonically treated at room temperature prior to the deposition.

2.2. Sb_2Se_3 film deposition

Commercial fluorine-doped SnO_2 (FTO) coated soda-lime glass (TEC 10, NSG, US) was cleaned with detergent, acetone, isopropanol, and deionized water in sequence in the ultrasonic bath. CdS window layer was deposited on the cleaned FTO glass via a chemical bath deposition as reported elsewhere (Guo et al., 2018). The Sb_2Se_3 thin films with 1 μm-thickness were grown in a close space sublimation (CSS) system under vacuum with deposition pressure of ~ 10 mTorr, where the top and bottom heaters were controlled at 300 and 550 °C for deposition, respectively. After Sb_2Se_3 film deposition, the CSS system was switched off to naturally cool down the system. NiO_x HTLs were deposited via spin coating with various spinning speeds (500 to 5000 rpm) for 30 s to control the film thickness. After spin coating, the NiO_x coated samples were dried on a hotplate in the air at 80 °C for 5 mins.

2.3. Materials characterization

The thickness of the Sb_2Se_3 films was estimated by the surface profilometer (KLA Tencor D-500) and validated by the SEM cross-section image. The crystal structure of NiO_x nanopowder and Sb_2Se_3 films were characterized by X-ray diffraction (XRD) system (Philips X'Pert) with Cu Kα radiation. The film morphology and chemical composition were characterized by the scanning electron microscope (SEM, JEOL 7000) and energy-dispersive spectroscopy (EDS) attached to the SEM. X-ray photoelectron spectroscopy (XPS) was collected using the Kratos Axis 165 XPS with Al source. The transmittance spectra were characterized by UV–Vis spectroscopy (Shimadzu UV1800).

2.4. Solar cell fabrication and measurement

The NiO_x HTLs were spin-coated on the as-deposited Sb_2Se_3 films with various thicknesses by manipulating the spin rotation speed. Au electrode was deposited using a shadow mask (area 0.09 cm^2) via the sputtering system with a 2 in. Au target. The current density–voltage (*J-V*) curve of the fabricated solar cells was characterized using a solar simulator (Newport, Oriel Class AAA 94063A, 1000 Watt Xenon light source) with a source meter (Keithley 2420) at 100 mW cm^{-2} AM 1.5 G irradiation. A calibrated Si-reference cell and meter (Newport, 91150 V, certified by NREL) was used to calibrate the solar simulator prior to the measurement. External Quantum Efficiency (EQE) of solar cells was obtained by the solar cell spectra response measurement system (QE-T, Enli Technology, Co. Ltd). Capacitance-Voltage (*C-V*) measurement was performed in the dark at room temperature using a Solartron Analytical 1260 impedance analyzer equipped with a 1296 dielectric interface at a frequency of 10 kHz, and the AC amplitude was 30 mV. DC bias was swept from −1 to 0.3 V. Electrochemical impedance spectroscopy (EIS) measurement was conducted on Solartron Analytical 1260 impedance analyzer at a bias potential of 0.5 V in the dark with the frequency ranging from 10^2 to 10^6 Hz. A light-soaking test was performed in a home-made aging chamber with a 1 sun light source and temperature at ~ 85 °C.

3. Results and discussion

Fig. 1a shows the XRD pattern of the as-prepared NiO_x nanopowders. NiO_x solutions were synthesized by fully dispersing NiO_x nanoparticles into DIW in the ultrasonic bath (inset of Fig. 1a). The typical cubic structure of the NiO_x has been determined through the three (1 1 1), (2 0 0), and (2 2 0) XRD peaks with 2 theta degrees of 37.2°, 43.2°, and 62.7°, respectively (Jin et al., 2018). The nanoparticle size has been calculated to be ~ 8 nm using the Scherrer equation, $\tau = K\lambda/\beta cos\theta$, where τ is the crystalline size, *K* is the shape factor (~0.9), β is the line broadening at half the maximum intensity (FWHM), and θ is the Bragg angle. The elemental composition of the deposited NiO_x films was characterized by XPS. Fig. 1b and 1c are high-resolution XPS spectra of Ni 2p and O 1 s core levels and the corresponding fitted results of Gaussian-Lorentzian curves after subtraction of a Shirley baseline, respectively. The strong peaks that appear at a binding energy of 854.1 eV (Fig. 1b) and 529.3 eV (Fig. 1c) are assigned to Ni^{2+} and O^{2-} states in the standard Ni-O octahedral bonding configuration in cubic rock-salt nickel oxide, respectively. In the high binding energy region, the peak observed at 855.8 eV is designated to the Ni^{3+} in Ni_2O_3 and NiOOH as a result of the Ni^{2+} vacancy. This indicates the as-deposited NiO_x is non-stoichiometric with abundant Ni^{2+} vacancies, which renders the as-prepared NiO_x with a desired hole transporting ability (Jin et al.,

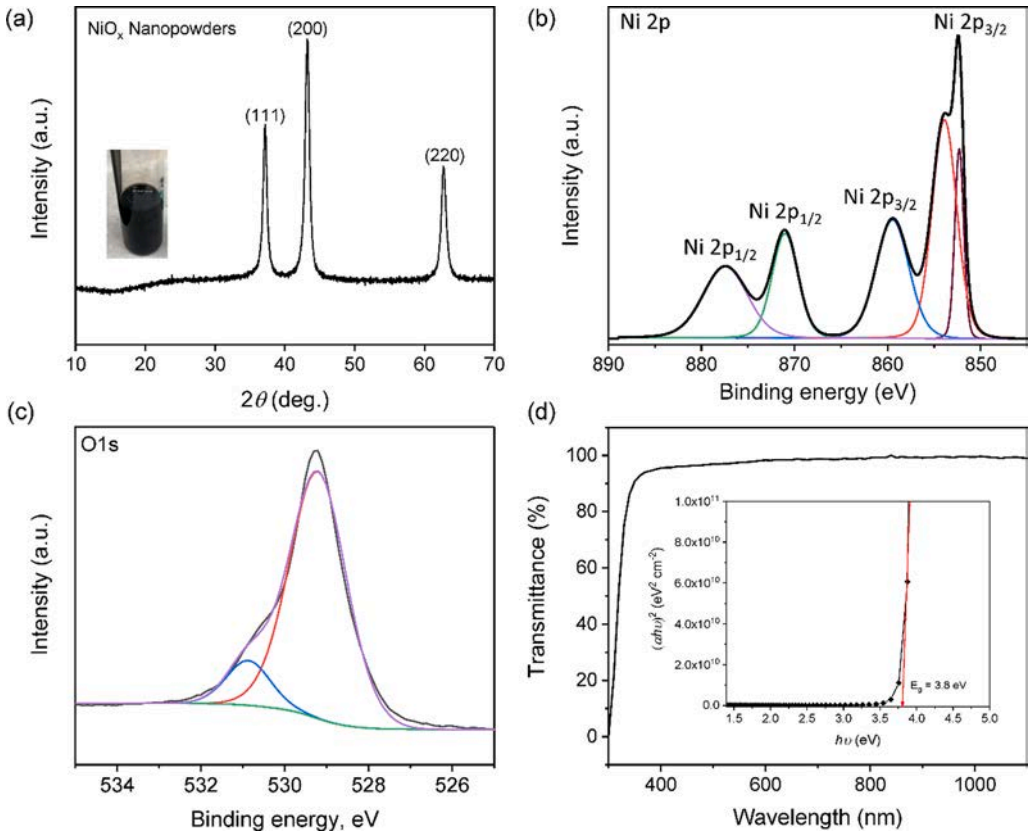

Fig. 1. (a) XRD pattern of the as-prepared NiO_x nanoparticles and the inset is the optical image of NiO_x ink. (b) XPS of Ni $2P_{3/2}$ and (c) O 1s core level for NiO_x film. (d) The transmittance of NiO_x film with Tauc plot inserted.

2018). The transmittance of the NiO_x film spin-coated on the glass substrate was characterized by the UV–Vis system, as shown in Fig. 1d. The as-deposited NiO_x film (~50 nm) shows a high transmittance of over 93% in the region of ~ 350 to 1100 nm, suggesting that the NiOx films have limited light absorption and may not impact the light absorption of the Sb_2Se_3 absorber. The bandgap derived from the transmittance shown in the inset of Fig. 1d indicates the as-deposited NiO_x film exhibits a wide bandgap of 3.8 eV.

To ascertain the coverage of the NiO_x on the Sb_2Se_3 film and the NiO_x/Sb_2Se_3 interface, we used the SEM equipped with EDS to characterize the NiO_x coated Sb_2Se_3 films. As shown in Fig. 2a-b, the as-deposited pristine Sb_2Se_3 film with thickness ~ 1 μm exhibits columnar rod-structured grains with ~ 300 nm on average, which could be associated with the orthorhombic crystal structure of the Sb_2Se_3.

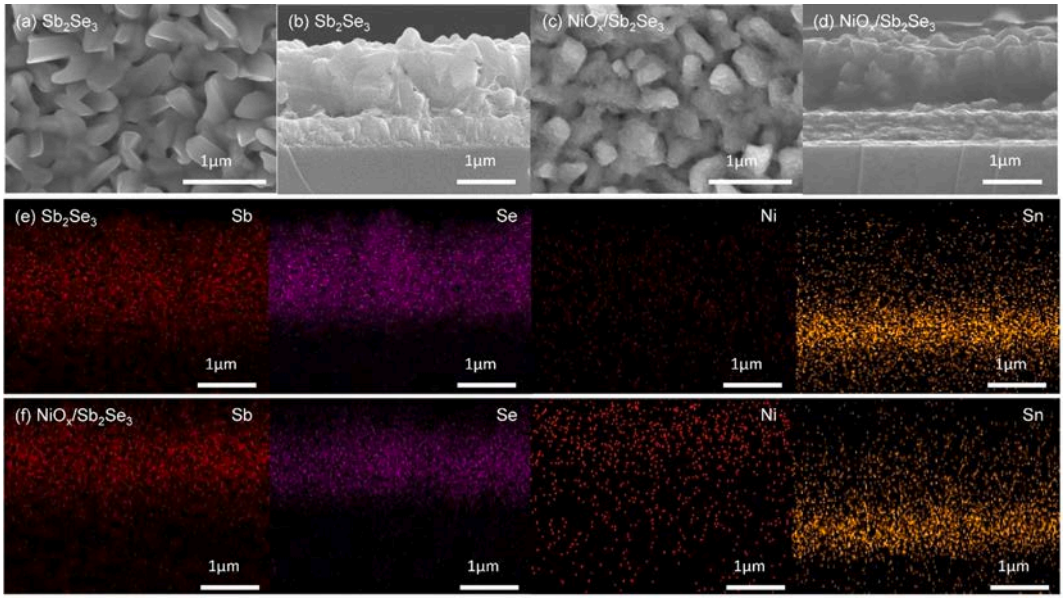

Fig. 2. Top-view SEM images of (a) pristine Sb_2Se_3 and (c) NiO_x coated Sb_2Se_3 films. Cross-sectional SEM images of (b) Sb_2Se_3 and (d) NiO_x/Sb_2Se_3 with the corresponding EDS elemental mapping images of constituent elements.

Particularly, the as-deposited Sb_2Se_3 presents a rough surface with clear voids on the surface, which may damage the interface between Sb_2Se_3 and the back contact. The atomic ratio of Se to Sb is close to 1.5 (60.36:39.64) determined by the EDS. The NiO_x nanoparticles coating on the Sb_2Se_3 film is uniform but still preserves a slightly columnar structure, as indicated in Fig. 2c-d. Especially, the NiO_x could effectively fill the voids on the surface of the as-deposited Sb_2Se_3, which could significantly impact the photogenerated carrier transport in the interface of Sb_2Se_3 and Au back contact. The corresponding EDS mapping for the cross-section of the Fig. 2b and 2d are shown in Fig. 2e and 2f, respectively, and it is shown that the NiO_x is uniformly spread on the top of the Sb_2Se_3 layer.

To investigate the effect of the NiO_x hole transport properties in the Sb_2Se_3 solar cells, Au electrodes with ~ 80 nm thickness were sputtered on the Sb_2Se_3 and NiO_x coated Sb_2Se_3 films to form a solar cell device in a superstrate configuration: FTO/CdS/Sb_2Se_3/NiO_x/Au, as shown in Fig. 3a. The energy band diagram of the device is plotted in Fig. 3b, where the NiO_x could promote the hole collection in the backside and block the electron transport to the back contact. This electron reflecting role is similar to the ZnTe back contact for the CdTe solar cells to make an ohmic contact (Niles et al., 1992), which could increase the photogenerated collection and prevent the electron recombination in the backside of the Sb_2Se_3 cells. As expected, the device performances extracted from the current density–voltage (*J-V*) curves (Fig. 3c) demonstrate that the NiO_x HTL can effectively improve the PCE to 7.29% with both increased open-circuit voltage and short circuit current. The detailed device parameters are summarized in Table 1. The NiO_x thickness optimization to achieve the best device performance will be discussed in detail later.

The incorporation of NiO_x HTL in the Sb_2Se_3 device directly enhances the EQE throughout the entire visible spectrum, as shown in Fig. 3d. Particularly, both the short and long wavelength light absorption became stronger, suggesting that the NiO_x HTL promotes the light conversion to electrons and holes and also through the electron reflection and hole collection via the desired band alignment as shown in Fig. 3b. The integrated J_{SC} of solar cells with/without NiO_x are 26.36 and 25.12 mA/cm^2, respectively, suggesting that the NiO_x could effectively extract the photogenerated holes. However, the integrated Jsc from EQE is lower than that of the Jsc values from the *J-V* curves (~10% lower). This Jsc offset between the EQE and *J-V* measurement is normally associated with the interface quality of the Sb_2Se_3 and the back contact. Here, we employ sputtering deposition of Au electrode, which has stronger ionic energy during deposition and may damage the Sb_2Se_3 and NiOx/Sb_2Se_3 surface compared to the traditional thermal evaporation deposited Au electrode. Therefore, it is expected that the EQE is more sensitive to the interface quality. The interface quality using the sputtered Au electrode on Sb_2Se_3 will be investigated in the future.

Table 1
Champion Device parameters of Sb_2Se_3 solar cells with and without NiO_x HTL.

Samples	Voc, V	Jsc, mA/cm^2	FF, %	PCE, %
Without NiOx	0.40	29.62	55.63	6.64
With NiO	0.41	30.94	57.26	7.29

To screen the optimal thickness of the NiO_x HTL, we deposited NiO_x on the Sb_2Se_3 film with varying rotation speed ranging from 0 to 5000 rpm to obtain different thicknesses (Fig. 4a). Fig. 4a shows the statistical distribution of the PCE with different NiO_x thicknesses. Note that the device performance increases with increasing NiO_x thickness from 0 nm to 50 nm from an average PCE of 6.12% to 7.15%, while PCE decreases with further increase in the NiO_x thickness to100 nm with an average PCE of 5.2%. Particularly, the change of Jsc and FF is consistent with the NiO_x thickness variation and dominates the device performance improvement. It is observed that the Voc was significantly improved with the insertion of 50 nm NiO_x, suggesting an improved hole collection via an optimized band alignment between Sb_2Se_3/NiO_x/Au. Also, incorporation of the NiO_x HTL in solar cells also boosts J_{SC} owing to the enhanced photogenerated current generation as shown in the EQE curve

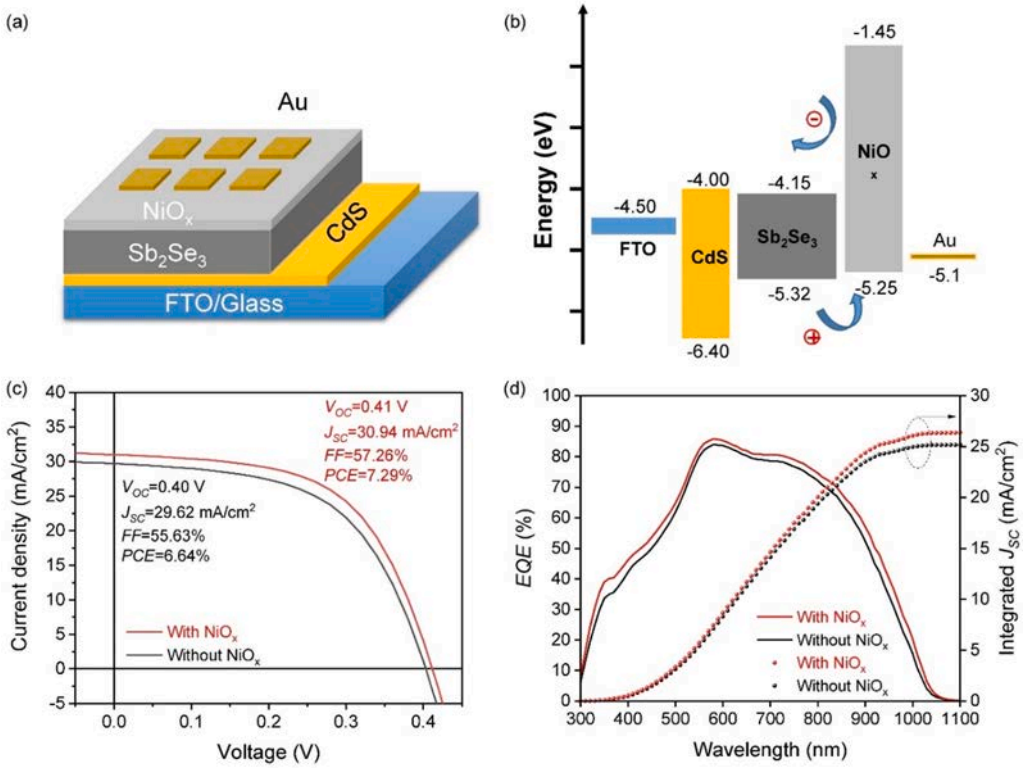

Fig. 3. (a) Schematic illustration of Sb_2Se_3 device configuration (b) Schematic of the energy band diagram of the Sb_2Se_3 cells with NiO_x hole transport layer. (c) *J-V* curves and (d) EQE spectra of the champion Sb_2Se_3 cells with and without NiO_x layer.

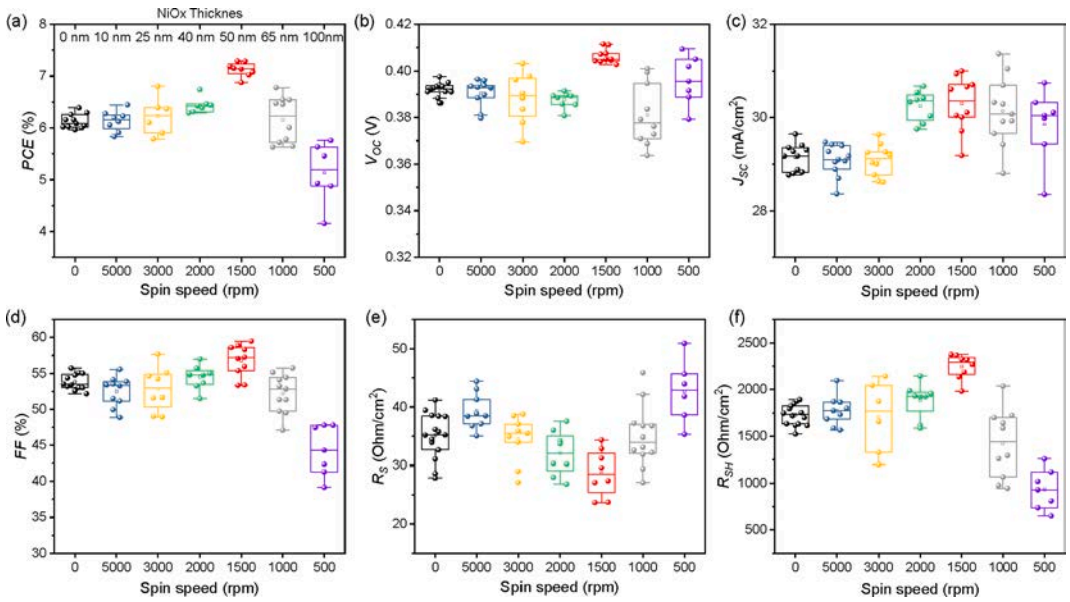

Fig. 4. Statistical distributions of (a) *PCE*, (b) V_{OC}, (c) J_{SC}, (d) *FF*, (e) R_S, and (f) R_{SH} of Sb_2Se_3 solar cells with NiO_x as the HTL with various thickness by tailoring spin coating rotation speed (Thickness are indexed in Fig. 4a).

in the full visible sunlight spectrum and better quality of interfaces among Sb_2Se_3/NiO_x/Au. Particularly, the series resistivity (*Rs*) of the device with NiO_x thickness less than 50 nm is gradually reduced, which contributes to the improved average FF up to 57.3%. With a thicker NiO_x HTLs of more than 50 nm, it is shown that the Rs greatly increases, leading to reduced PCE, FF, Jsc, and shunting resistivity (R_{sh}). It is expected that the thick NiO_x may block the photoinduced holes collection by the Au electrode.

To determine the carrier concentration and the carrier transport capability in the Sb_2Se_3 device with NiO_x HTL, the *C-V* measurement was performed. Fig. 5a. shows the Mott-Schottky plot of both the Sb_2Se_3 solar cell devices with and without NiO_x. It is observed that the built-in potential (V_{bi}) is about 0. 32 V for both devices, which indicates that the NiO_x HTL may not change the V_{bi} too much and in agreement with only slightly improved Voc. However, at the 0 V bias, the capacitance of the Sb_2Se_3 device with NiO_x possesses a smaller capacitance value than that

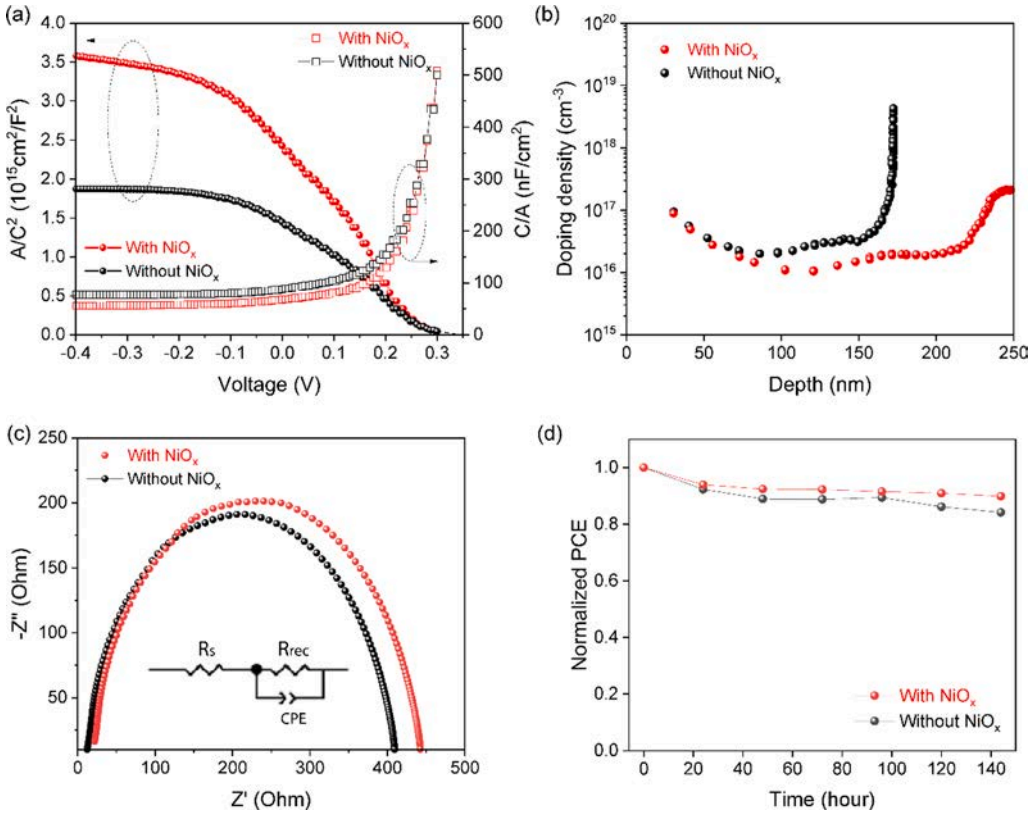

Fig. 5. (a) A/C^2 and C/A versus applied voltage (V) graphs; (b) logarithmic representation of a C-V derived carrier density profiles, and (c) Nyquist plots for the Sb_2Se_3 cells with and without NiO_x hole transport layer. (d) Light soaking stability test (85 °C, 1 sun solar simulator).

of the device without NiOx. The width of the depletion region of the devices can be determined through the capacitance–voltage formula, $W = A\varepsilon\varepsilon_0/C_0$, where A is electrode area, ε is the permittivity, ε_0 is the vacuum permittivity, and C_0 is the capacitance at 0 V bias (Yan, 2018). The calculated width of the depletion region is shown in Fig. 5b, where the NiO_x HTL significantly improved the depletion region from 165 nm to 225 nm compared to that of the device without NiO_x. The increased depletion region could be ascribed to the formed n-i-p heterojunction, which benefits the carrier generation and extraction (Guo et al., 2019). The charge carrier density (N_{CV}) profile as a function of the distance from the junction is calculated based on the equation: $N_{CV}(D) = \frac{2}{q\varepsilon A^2}\left[\frac{dC(V)^{-2}}{dV}\right]^{-1}$, where q is the electron charge, ε is the semiconductor permittivity, A is the cell area, and $\frac{dC(V)^{-2}}{dV}$ is the slope of the curve C^{-2}-V curve shown in Fig. 5(a). D is the depth of the junction, which can be calculated from $D=\frac{\varepsilon A}{C}$. Fig. 5(b) shows the *C-V* doping profiling for the devices with and without NiO_x. Particularly, the NiO_x HTL did not impact the hole density in the devices, which is $\sim 2 \times 10^{16}$ cm^{-3} at 0 V bias, suggesting that the Ni or O ions may not diffuse into the device as dopants.

To better understand the role of NiO_x on the interface charge transport, EIS was employed to characterize the Sb_2Se_3 devices with and without NiO_x HTL. Fig. 5c shows the Nyquist plots of the devices with/without the NiO_x HTL. An equivalent circuit (inset of Fig. 5c) with series resistance (Rs), a charge recombination resistance (Rrec), and a constant phase angle element (CPE) was used to fit the semicircle. The fitting results are shown in Table 2 Since the CdS, Sb_2Se_3, and Au electrodes are the same in both devices, the variation of the semicircle may originate from the interface of $Sb_2Se_3/NiO_x/Au$, where a larger Rrec suggests a lower charge recombination interface with NiO_x HTL. In other words, NiO_x HTL could effectively suppress the carrier recombination at the backside of the Sb_2Se_3 device. To evaluate the stability with the NiO_x HTL of the Sb_2Se_3 solar cells, an accelerated stress test of the device stability under light soaking at 85 °C and 1 sun (100 mW cm^{-2}) was carried out (Fig. 5d). Overall, the Sb_2Se_3 device with/without NiO_x retains 80% of the initial efficiency after about 140 h, suggesting both devices show good stability under accelerated stress. Particularly, with the NiO_x HTL, the degradation rate for the device is slower compared to that of the device without NiO_x, indicating that NiO_x HTL could improve device stability.

4. Conclusions

In summary, NiO_x as an effective HTL for Sb_2Se_3 thin-film solar cells has been demonstrated. NiO_x nanoparticle was successfully synthesized to form NiO_x ink, which can be directly spin-coated on the Sb_2Se_3 films at a low cost. NiO_x HTL can significantly improve the device performance of the Sb_2Se_3 solar cells from PCE of 6.12% to 7.15% by tailoring the NiO_x thickness. NiO_x HTL not only enhances the carrier collection via the electron reflection effect but also suppresses carrier recombination at the $Sb_2Se_3/NiO_x/Au$ interface. This work provides a cost-effective, nontoxic hole-transporting material for Sb_2Se_3 solar cells, which paves the way to further developing more efficient Sb_2Se_3 solar cells by the introduction of hole transport materials.

Author contributions

Prof. Feng Yan designed the research and Liping Guo, N. Vijayaraghavan, Xiaomeng Duan- and Harigovind G. Menon performed research, analyzed data, and revised the manuscript. Prof. Lingyan Kong, Subhadra Gupta, and. Lin Li helped performed research and review & edit the manuscript.

Table 2
Fitting parameters of EIS results by using a R(CR) equivalent circuit.

Samples	Rs, Ω cm^2	CPE, F/cm^2	Rrec, Ω cm^2	CPE-P
Without NiO_x	17.6	2.53×10^{-8}	392.5	0.94
With NiO_x	15.9	1.31×10^{-8}	594.5	0.94

Declaration of Competing Interest

The authors declare that they have no known competing financial interests or personal relationships that could have appeared to influence the work reported in this paper.

Acknowledgments

This work is supported by National Science Foundation under contract No. 1944374 and 2019473, National Aeronautics and Space Administration, Alabama EPSCoR International Space Station Flight Opportunity program (contract# 80NSSC20M0141), and USDA National Institute of Food and Agriculture, AFRI project award (contract# 2020-67022-31376).

References

Chen, C., Tang, J., 2020. Open-Circuit Voltage Loss of Antimony Chalcogenide Solar Cells: Status, Origin, and Possible Solutions. ACS Energy Lett. 5 (7), 2294–2304.
Chen, C., Wang, L., Gao, L., Nam, D., Li, D., Li, K., Zhao, Y., Ge, C., Cheong, H., Liu, H., Song, H., Tang, J., 2017. 6.5% Certified Efficiency Sb 2 Se 3 Solar Cells Using PbS Colloidal Quantum Dot Film as Hole-Transporting Layer. ACS Energy Lett. 2 (9), 2125–2132.
Choi, Y.C., Mandal, T.N., Yang, W.S., Lee, Y.H., Im, S.H., Noh, J.H., Seok, S.I., 2014. Sb 2 Se 3 -Sensitized Inorganic-Organic Heterojunction Solar Cells Fabricated Using a Single-Source Precursor. Angew. Chem. Int. Ed. 53 (5), 1329–1333.
Crabtree, G.W., Lewis, N.S., 2007. Solar energy conversion. Physics Today 60 (3), 37–42.
Green, M.A., Bremner, S.P., 2017. Energy conversion approaches and materials for high-efficiency photovoltaics. Nature Mater 16 (1), 23–34.
Green, M.A., Dunlop, E.D., Levi, D.H., Hohl-Ebinger, J., Yoshita, M., Ho-Baillie, A.W.Y., 2019. Solar cell efficiency tables (version 54). Prog Photovolt Res Appl 27 (7), 565–575.
Guijarro, N., Lutz, T., Lana-Villarreal, T., O'Mahony, F., Gómez, R., Haque, S.A., 2012. Toward Antimony Selenide Sensitized Solar Cells: Efficient Charge Photogeneration at spiro -OMeTAD/Sb 2 Se 3 /Metal Oxide Heterojunctions. J. Phys. Chem. Lett. 3 (10), 1351–1356.
Guo, L., Zhang, B., Qin, Y., Li, D., Li, L., Qian, X., Yan, F., 2018. Tunable Quasi-One-Dimensional Ribbon Enhanced Light Absorption in Sb 2 Se 3 Thin-film Solar Cells Grown by Close-Space Sublimation. Sol. RRL 2 (10), 1800128. https://doi.org/10.1002/solr.v2.1010.1002/solr.201800128.
Guo, L., Zhang, B., Ranjit, S., Wall, J., Saurav, S., Hauser, A.J., Xing, G., Li, L., Qian, X., Yan, F., 2019. Interface Engineering via Sputtered Oxygenated CdS:O Window Layer for Highly Efficient Sb 2 Se 3 Thin-Film Solar Cells with Efficiency Above 7%. Sol. RRL 3 (10), 1900225. https://doi.org/10.1002/solr.v3.1010.1002/solr.201900225.
Hobson, T.D.C., Phillips, L.J., Hutter, O.S., Shiel, H., Swallow, J.E.N., Savory, C.N., Nayak, P.K., Mariotti, S., Das, B., Bowen, L., Jones, L.A.H., Featherstone, T.J., Smiles, M.J., Farnworth, M.A., Zoppi, G., Thakur, P.K., Lee, T.-L., Snaith, H.J., Leighton, C., Scanlon, D.O., Dhanak, V.R., Durose, K., Veal, T.D., Major, J.D., 2020. Isotype Heterojunction Solar Cells Using n-Type Sb 2 Se 3 Thin Films. Chem. Mater. 32 (6), 2621–2630.
Jin, X., Yuan, Y., Jiang, C., Ju, H., Jiang, G., Liu, W., Zhu, C., Chen, T., 2018. Solution processed NiOx hole-transporting material for all-inorganic planar heterojunction Sb2S3 solar cells. Solar Energy Materials and Solar Cells 185, 542–548.
Ju, T., Koo, B., Jo, J.W., Ko, M.J., 2020. Enhanced photovoltaic performance of solution-processed Sb2Se3 thin film solar cells by optimizing device structure. Current Applied Physics 20 (2), 282–287.
Kamruzzaman, M., Liu, C., Farid Ul Islam, A.K.M., Zapien, J.A., 2017. A comparative study on the electronic and optical properties of Sb2Se3 thin film. Semiconductors 51 (12), 1615–1624.
Lee, S., Lee, J., Park, H., Choi, J., Baac, H.W., Park, S., Park, H.J., 2020. Defect-Passivating Organic/Inorganic Bicomponent Hole-Transport Layer for High Efficiency Metal-Halide Perovskite Device. ACS Appl. Mater. Interfaces 12 (36), 40310–40317.
Li, D.-B., Yin, X., Grice, C.R., Guan, L., Song, Z., Wang, C., Chen, C., Li, K., Cimaroli, A.J., Awni, R.A., Zhao, D., Song, H., Tang, W., Yan, Y., Tang, J., 2018. Stable and efficient CdS/Sb2Se3 solar cells prepared by scalable close space sublimation. Nano Energy 49, 346–353.
Li, K., Wang, S., Chen, C., Kondrotas, R., Hu, M., Lu, S., Wang, C., Chen, W., Tang, J., 2019a. 7.5% n–i–p Sb 2 Se 3 solar cells with CuSCN as a hole-transport layer. J. Mater. Chem. A 7 (16), 9665–9672.
Li, Z., Liang, X., Li, G., Liu, H., Zhang, H., Guo, J., Chen, J., Shen, K., San, X., Yu, W., Schropp, R.E.I., Mai, Y., 2019b. 9.2%-efficient core-shell structured antimony

selenide nanorod array solar cells. Nat Commun 10 (1). https://doi.org/10.1038/s41467-018-07903-6.

Messina, S., Nair, M.T.S., Nair, P.K., 2009. Antimony Selenide Absorber Thin Films in All-Chemically Deposited Solar Cells. J. Electrochem. Soc. 156 (5), H327. https://doi.org/10.1149/1.3089358.

Niles, D.W., Höchst, H., Rioux, D., 1992. Valence band discontinuity at the ZnTe/CdTe interface: Making ohmic contact to P-type CdTe. AIP Conference Proceedings 268 (1), 279–284.

Park, J.H., Seo, J., Park, S., Shin, S.S., Kim, Y.C., Jeon, N.J., Shin, H.-W., Ahn, T.K., Noh, J.H., Yoon, S.C., Hwang, C.S., Seok, S.I., 2015. Efficient CH 3 NH 3 PbI 3 Perovskite Solar Cells Employing Nanostructured p-Type NiO Electrode Formed by a Pulsed Laser Deposition. Adv. Mater. 27 (27), 4013–4019.

Tang, R., Wang, X., Lian, W., Huang, J., Wei, Q.i., Huang, M., Yin, Y., Jiang, C., Yang, S., Xing, G., Chen, S., Zhu, C., Hao, X., Green, M.A., Chen, T., 2020. Hydrothermal deposition of antimony selenosulfide thin films enables solar cells with 10% efficiency. Nat Energy 5 (8), 587–595.

Wong, L.H., Zakutayev, A., Major, J.D., Hao, X., Walsh, A., Todorov, T.K., Saucedo, E., 2019. Emerging inorganic solar cell efficiency tables (Version 1). J. Phys.: Energy 1, 3, 032001.

Xu, X., Liu, Z., Zuo, Z., Zhang, M., Zhao, Z., Shen, Y., Zhou, H., Chen, Q., Yang, Y., Wang, M., 2015. Hole selective NiO contact for efficient perovskite solar cells with carbon electrode. Nano Lett 15, 4, 2402–2408.

Yan, R.A.A.C.R.G.D.-b.L.Z.S.Y., 2018. Electrical Impedance Characterization of CdTe. 2018 IEEE 7th World Conference on Photovoltaic Energy Conversion 1878.

Yin, Xingtian, Chen, Peng, Que, Meidan, Xing, Yonglei, Que, Wenxiu, Niu, Chunming, Shao, Jinyou, 2016. Highly Efficient Flexible Perovskite Solar Cells Using Solution-Derived NiO x Hole Contacts. ACS Nano 10 (3), 3630–3636.

You, Jingbi, Meng, Lei, Song, Tze-Bin, Guo, Tzung-Fang, Yang, Yang (Michael), Chang, Wei-Hsuan, Hong, Ziruo, Chen, Huajun, Zhou, Huanping, Chen, Qi, Liu, Yongsheng, De Marco, Nicholas, Yang, Yang, 2016. Improved air stability of perovskite solar cells via solution-processed metal oxide transport layers. Nat. Nanotech. 11 (1), 75–81.

Zeng, Kai, Xue, Ding-Jiang, Tang, Jiang, 2016. Antimony selenide thin-film solar cells. Semicond. Sci. Technol. 31 (6), 063001. https://doi.org/10.1088/0268-1242/31/6/063001.

Zhang, Jun, Kondrotas, Rokas, Lu, Shuaicheng, Wang, Chong, Chen, Chao, Tang, Jiang, 2019. Alternative back contacts for Sb2Se3 solar cells. Sol. Energy 182, 96–101.

Zhou, Ying, Leng, Meiying, Xia, Zhe, Zhong, Jie, Song, Huaibing, Liu, Xinsheng, Yang, Bo, Zhang, Junpei, Chen, Jie, Zhou, Kunhao, Han, Junbo, Cheng, Yibing, Tang, Jiang, 2014. Solution-Processed Antimony Selenide Heterojunction Solar Cells. Adv. Energy Mater. 4 (8), 1301846. https://doi.org/10.1002/aenm.201301846.

Zhou, Ying, Wang, Liang, Chen, Shiyou, Qin, Sikai, Liu, Xinsheng, Chen, Jie, Xue, Ding-Jiang, Luo, Miao, Cao, Yuanzhi, Cheng, Yibing, Sargent, Edward H., Tang, Jiang, 2015. Thin-film Sb2Se3 photovoltaics with oriented one-dimensional ribbons and benign grain boundaries. Nature Photon 9 (6), 409–415.

Zhu, Z., Bai, Y., Zhang, T., Liu, Z., Long, X., Wei, Z., Wang, Z., Zhang, L., Wang, J., Yan, F., Yang, S., 2014. High-performance hole-extraction layer of sol-gel-processed NiO nanocrystals for inverted planar perovskite solar cells. Angew. Chem. Int. Ed. Engl. 53 (46), 12571–12575.